A simple and accurate approximation for the Q stability parameter in multicomponent and realistically thick discs

Alessandro B. Romeo* and Niklas Falstad

Department of Earth and Space Sciences, Chalmers University of Technology, Onsala Space Observatory, SE-43992 Onsala, Sweden

ABSTRACT

In this paper, we propose a Q stability parameter that is more realistic than those commonly used, and is easy to evaluate (see equation 19). Using our $\mathcal{Q}_N$ parameter, you can take into account several stellar and/or gaseous components as well as the stabilizing effect of disc thickness, you can predict which component dominates the local stability level, and you can do all that simply and accurately. To illustrate the strength of $\mathcal{Q}_N$, we analyse the stability of a large sample of spirals from The H I Nearby Galaxy Survey (THINGS), treating stars, H I and H$_2$ as three distinct components. Our analysis shows that H$_2$ plays a significant role in disc (in)stability even at distances as large as half the optical radius. This is an important aspect of the problem, which was missed by previous (two-component) analyses of THINGS spirals. We also show that H I plays a negligible role up to the edge of the optical disc and that the stability level of THINGS spirals is, on average, remarkably flat and well above unity.

Key words: instabilities – stars: kinematics and dynamics – ISM: kinematics and dynamics – galaxies: ISM – galaxies: kinematics and dynamics – galaxies: star formation.

1 INTRODUCTION

Today, several decades after the pioneering work of Lin & Shu (1966) and the seminal papers by Jog & Solomon (1984a,b), it is widely accepted that stars and cold interstellar gas have an important interplay in the gravitational instability of galactic discs. The gravitational coupling between stars and gas does not alter the form of the local axisymmetric stability criterion, $Q \geq 1$ (Toomre 1964), but makes the Q stability parameter dependent on the radial velocity dispersions and surface mass densities of the two components (Bertin & Romeo 1988; Elmegreen 1995; Jog 1996; Rafikov 2001; Shen & Lou 2003). The value of Q is also affected by other factors, such as the vertical structure of the disc (Shu 1968; Romeo 1990, 1992, 1994; Elmegreen 2011; Romeo & Wiegert 2011), gas turbulence (Hoffmann & Romeo 2012; Shadmehri & Khajenabi 2012) and gas dissipation (Elmegreen 2011). Comprehensive analyses have shown that the two-component Q parameter has a large impact on the dynamics and evolution of spiral structure in galaxies (see Bertin & Lin 1996), and is also a useful diagnostic for exploring the link between disc instability and star formation (Leroy et al. 2008).

Romeo & Wiegert (2011) introduced a simple and accurate approximation for the two-component Q parameter, which takes into account the stabilizing effect of disc thickness and predicts whether the local stability level is dominated by stars or gas. The Romeo–Wiegert approximation has been used for investigating the evolution

of gravitationally unstable discs (Cacciato, Dekel & Genel 2012; Forbes, Krumholz & Burkert 2012), the spiral structure of NGC 5247 (Khoperskov et al. 2012), the dynamical link between dark matter and H I in nearby galaxies (Meurer, Zheng & de Blok 2013), as well as the link between disc stability and the relative distributions of stars, gas and star formation (Zheng et al. 2013). Forbes et al. (2012) concluded that the Romeo–Wiegert approximation is much faster to use than the Q stability parameter of Rafikov (2001): it speeds up their disc-evolution code by as much as one or two orders of magnitude! This is simply because such an approximation estimates Q analytically, without the need to minimize the dispersion relation over all wavenumbers, as is usually done.

A fundamental problem that must be faced when analysing the stability of galactic discs is how to represent their complex structure using only two components. The results of such analyses are indeed very sensitive to the choice of the gaseous 1D velocity dispersion, σ_g: the colder the gas, the stronger its impact on the stability of the disc (e.g. Jog & Solomon 1984a; Bertin & Romeo 1988). Choosing $\sigma_g \approx 6\,\mathrm{km\,s^{-1}}$ will represent molecular gas well (Wilson et al. 2011), but will overestimate the contribution of atomic gas and make the disc more unstable than it actually is. Vice versa, choosing $\sigma_g \approx 11\,\mathrm{km\,s^{-1}}$ will represent H I well (Leroy et al. 2008), but will underestimate the contribution of H$_2$ and stabilize the disc artificially. Intermediate values or more elaborate choices of σ_g will still not solve the problem. This motivates the use of a proper multicomponent Q parameter.

One of the first papers that discussed the gravitational instability of multicomponent discs dates back to Morozov (1981). This author derived a dispersion relation that is valid for infinitesimally thin

---

* E-mail: romeo@chalmers.se

discs made of gas and N_* stellar components. He also calculated the stability criterion for $N_* = 2$. Rafikov (2001) derived a stability criterion that is valid for any N_* and can easily be expressed in the usual form $Q \geq 1$.[1]

In this paper, we introduce a new Q stability parameter, which has the same strong advantages as the Romeo–Wiegert approximation, and which is applicable to fully multicomponent and realistically thick discs (see equation 19). We also show how to use our $\mathcal{Q}_N$ parameter for analysing the stability of galactic discs, and illustrate the strength of a multicomponent analysis. We do so using a large sample of spirals from The H ɪ Nearby Galaxy Survey (THINGS), and treating stars, H ɪ and H_2 as three distinct components.

The rest of the paper is organized as follows. In Section 2, we review the basic case of two-component discs and further motivate the need for a multicomponent analysis (Section 2.1), we present our $\mathcal{Q}_N$ parameter (Sections 2.2– 2.4), and we analyse the stability of THINGS spirals (Section 2.5). In Section 3, we discuss the weaknesses of $\mathcal{Q}_N$, which are common to all Q parameters and stability criteria quoted here. In Section 4, we draw the conclusions.

2 STAR–GAS INSTABILITIES AND THE Q DIAGNOSTIC

2.1 Two components . . . or more? More!

Let us first discuss the case of two-component and infinitesimally thin discs, which is fundamental to a proper understanding of Sections 2.2–2.5. It is well known that the stability properties of such discs are determined by five basic quantities: the epicyclic frequency, κ, the stellar and gaseous surface densities, Σ_* and Σ_g, the stellar radial velocity dispersion, σ_{R*}, and the gaseous 1D velocity dispersion, σ_{1Dg} (e.g. Lin & Shu 1966; Rafikov 2001). The last two quantities reflect an important dynamical difference between stars and cold interstellar gas. The stellar component is collisionless so its velocity dispersion is anisotropic, while gas is collisional and has an isotropic velocity dispersion (see, e.g. Binney & Tremaine 2008). Hereafter, we will simplify the notation and denote the relevant velocity dispersions of the two components with σ_* and σ_g.

Lin & Shu (1966) and Rafikov (2001) took those facts into account by treating stars as a kinetic component and gas as a fluid (see also Shu 1968). The resulting local axisymmetric stability criteria are equivalent because they are based on the same dispersion relation, $\omega^2(k)$, and because they are derived by imposing that $\omega^2(k) \geq 0$ for all k. However, Rafikov's stability criterion is simpler and more used (e.g. Dalcanton, Yoachim & Bernstein 2004; Li, Mac Low & Klessen 2005, 2006; Kim & Ostriker 2007; Yang et al. 2007; Yim et al. 2011). Such a criterion can be written as $Q_{Rk} \geq 1$, where

$$\frac{1}{Q_{Rk}} = \max\{SC_{Rk}(K)\}, \tag{1}$$

$$SC_{Rk}(K) = \frac{1}{Q_*} \frac{2\left[1 - e^{-K^2} I_0\left(K^2\right)\right]}{K} + \frac{1}{Q_g} \frac{2Ks}{1 + K^2 s^2}, \tag{2}$$

$$K = k \frac{\sigma_*}{\kappa}, \tag{3}$$

$$Q_* = \frac{\kappa \sigma_*}{\pi G \Sigma_*}, \qquad Q_g = \frac{\kappa \sigma_g}{\pi G \Sigma_g}, \tag{4}$$

[1] Another (unpublished) stability analysis of N-component discs was made by Romeo (1985, pp. 140–145, 215–216).

$$s = \frac{\sigma_g}{\sigma_*}. \tag{5}$$

In these equations, Q_{Rk} is Rafikov's kinetic–fluid Q parameter, $SC_{Rk}(K)$ is the related stability curve, K is the radial wavenumber of the perturbation expressed in dimensionless form, Q_* and Q_g are the stellar and gaseous Toomre parameters and I_0 denotes the modified Bessel function of the first kind and order zero.

Bertin & Romeo (1988), Elmegreen (1995), Jog (1996) and again Rafikov (2001) adopted a less rigorous, but more straightforward approach: they treated the stellar component as a fluid, with sound speed equal to σ_*. The resulting two-fluid stability criteria are equivalent, apart from the different parametrizations used, because they are based on the same dispersion relation (Jog & Solomon 1984a). However, even in this case, Rafikov's criterion is simpler and is becoming more and more widely used (e.g. Leroy et al. 2008; Robertson & Kravtsov 2008; Dekel, Sari & Ceverino 2009; Mastropietro, Burkert & Moore 2009; Ceverino, Dekel & Bournaud 2010; Westfall et al. 2011; Elson, de Blok & Kraan-Korteweg 2012; Watson et al. 2012; Williamson & Thacker 2012). Such a criterion can be written as $Q_{Rf} \geq 1$, where Rafikov's fluid–fluid Q parameter can be computed by maximizing the related stability curve over all radial wavenumbers:

$$\frac{1}{Q_{Rf}} = \max\{SC_{Rf}(K)\}, \tag{6}$$

$$SC_{Rf}(K) = \frac{1}{Q_*} \frac{2K}{1 + K^2} + \frac{1}{Q_g} \frac{2Ks}{1 + K^2 s^2}. \tag{7}$$

What is the accuracy of the two-fluid stability criterion? Bertin & Romeo (1988) compared the fluid–fluid and kinetic–fluid marginal stability curves in a representative set of cases, and showed that the differences are small (see their fig. 2). Rafikov (2001) carried out a more detailed analysis and got similar results (see his fig. 3). However, he did not evaluate the relative error $(Q_{Rf} - Q_{Rk})/Q_{Rk}$, which depends on s and

$$q = \frac{Q_g}{Q_*}, \tag{8}$$

and which is a useful piece of information for assessing the accuracy of Q_{Rf}. We do this in Fig. 1. Our contour map shows that such error is less than 7 per cent and has a root-mean-square value of 4 per cent. This means that Q_{Rf} and Q_{Rk} are practically equivalent, since the parameters s and q are themselves subject to observational uncertainties.

Romeo & Wiegert (2011) showed that the two-fluid Q parameter can be accurately estimated without the usual maximization (or minimization) procedure:

$$\frac{1}{Q_{RW}} = \begin{cases} \dfrac{W}{Q_*} + \dfrac{1}{Q_g} & \text{if } Q_* \geq Q_g, \\[2ex] \dfrac{1}{Q_*} + \dfrac{W}{Q_g} & \text{if } Q_g \geq Q_*; \end{cases} \tag{9}$$

$$W = \frac{2\sigma_* \sigma_g}{\sigma_*^2 + \sigma_g^2}. \tag{10}$$

Although very recent, such an approximation is already frequently used (e.g. Cacciato et al. 2012; Forbes et al. 2012; Hoffmann & Romeo 2012; Khoperskov et al. 2012; Meurer et al. 2013; Zheng et al. 2013). Fig. 2 shows that Q_{RW} is remarkably accurate even with respect to the kinetic–fluid Q parameter. In fact, the relative error
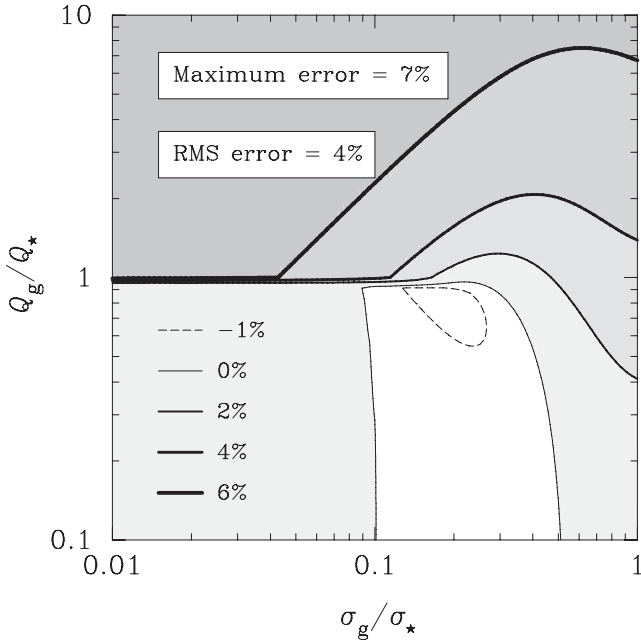
Figure 1. Accuracy of the two-fluid stability criterion. The curves shown are the contour lines of the relative error $(Q_{Rf} - Q_{Rk})/Q_{Rk}$, where Q_{Rf} and Q_{Rk} are the fluid–fluid and kinetic–fluid Q parameters of Rafikov (2001). In addition, Q_* and Q_g are the stellar and gaseous Toomre parameters, σ_* and σ_g are the relevant velocity dispersions of the two components.
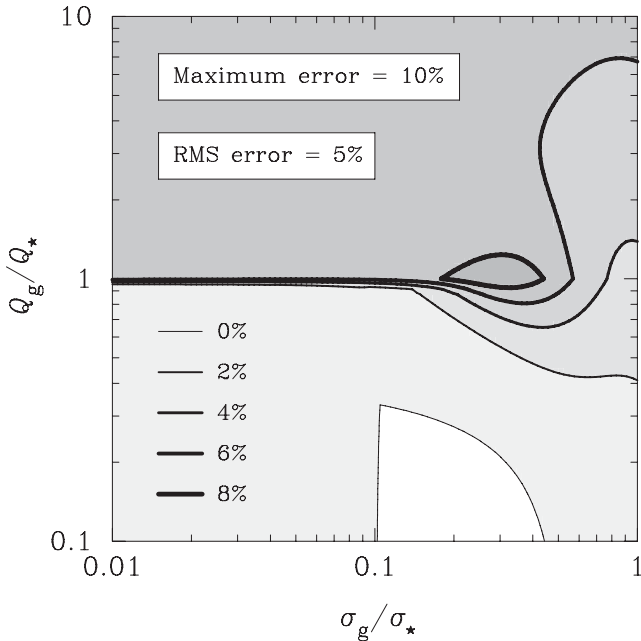
Figure 2. Accuracy of the Romeo–Wiegert approximation. The curves shown are the contour lines of the relative error $(Q_{RW} - Q_{Rk})/Q_{Rk}$, where Q_{RW} is the two-component Q parameter of Romeo & Wiegert (2011), and Q_{Rk} is the kinetic–fluid Q parameter of Rafikov (2001). The rest of the notation is the same as in Fig. 1.

$(Q_{RW} - Q_{Rk})/Q_{Rk}$ is below 10 per cent and has a root-mean-square value of 5 per cent. Thus Q_{RW} is a faster and physically equivalent alternative to Q_{Rf} or Q_{Rk}.

To understand the weaknesses of a two-component analysis, let us see how spiral galaxies populate the parameter plane of star–gas

instabilities. We use a sample of 12 nearby star-forming spirals from THINGS, previously analysed by Leroy et al. (2008) and Romeo & Wiegert (2011): NGC 628, 2841, 3184, 3198, 3351, 3521, 3627, 4736, 5055, 5194, 6946 and 7331. For each galaxy of this sample, we compute the radial profiles $s = s(R)$ and $q = q(R)$, and hence the track left by the galaxy in the (s, q) plane. The result for the whole sample is shown in the left-hand panel of Fig. 3. Note that 20 per cent of the data fall within the shaded part of the (s, q) plane, which represents the condition for star–gas decoupling. In this region, $SC_{Rk}(K)$ has two maxima: one at small K, where the response of the stellar component peaks; and the other at large K, where gas dominates. In the 'stellar phase', the maximum at small K is higher than the other one, and therefore it controls the onset of disc instability. Vice versa, in the 'gaseous phase', it is the maximum at large K that determines Q_{Rk}. The two-fluid counterpart of this region (thin dashed lines) is also populated by 20 per cent of the data (Romeo & Wiegert 2011). In the rest of the parameter plane, the dynamical responses of the two components are strongly coupled and peak at a single wavelength.

The analysis of THINGS spirals carried out above treats the interstellar medium (ISM) as a single component with $\Sigma_g = \Sigma_{HI} + \Sigma_{H_2}$ and $\sigma_g = 11 \text{ km s}^{-1}$ (Leroy et al. 2008). What are the limitations of this approach? How do H I and H$_2$ contribute to star–gas instabilities? To answer these questions, we consider H I and H$_2$ separately, and choose observationally motivated values of the 1D velocity dispersion: $\sigma_{HI} = 11 \text{ km s}^{-1}$ (Leroy et al. 2008), and $\sigma_{H_2} = 6 \text{ km s}^{-1}$ (Wilson et al. 2011). We then compute the (s, q) tracks for each case (stars plus H I or H$_2$), and show the results in the right-hand panel of Fig. 3. Note that H I and H$_2$ populate the parameter plane differently. In particular, none of the H I data falls within the two-phase region, while H$_2$ populates such a region in 60 per cent of the cases. This means that H I and H$_2$ have distinct stability properties, and a fundamentally different dynamical coupling with stars. Treating the ISM as a single component underestimates the role that H$_2$ plays in star–gas instabilities, and overestimates the contribution of H I. This is why a multicomponent analysis is needed!

2.2 Approximating Q in the thin-disc limit

The only multicomponent stability diagnostics that have been available so far are the local axisymmetric stability criteria of Morozov (1981) and Rafikov (2001), which are valid for infinitesimally thin discs made of gas and N_* stellar components. For $N_* = 2$, the case considered by Morozov (1981), such criteria are equivalent because they are based on similar approximations. However, besides being more general, Rafikov's criterion is simpler and can be written as $Q_{R, N} \geq 1$, where
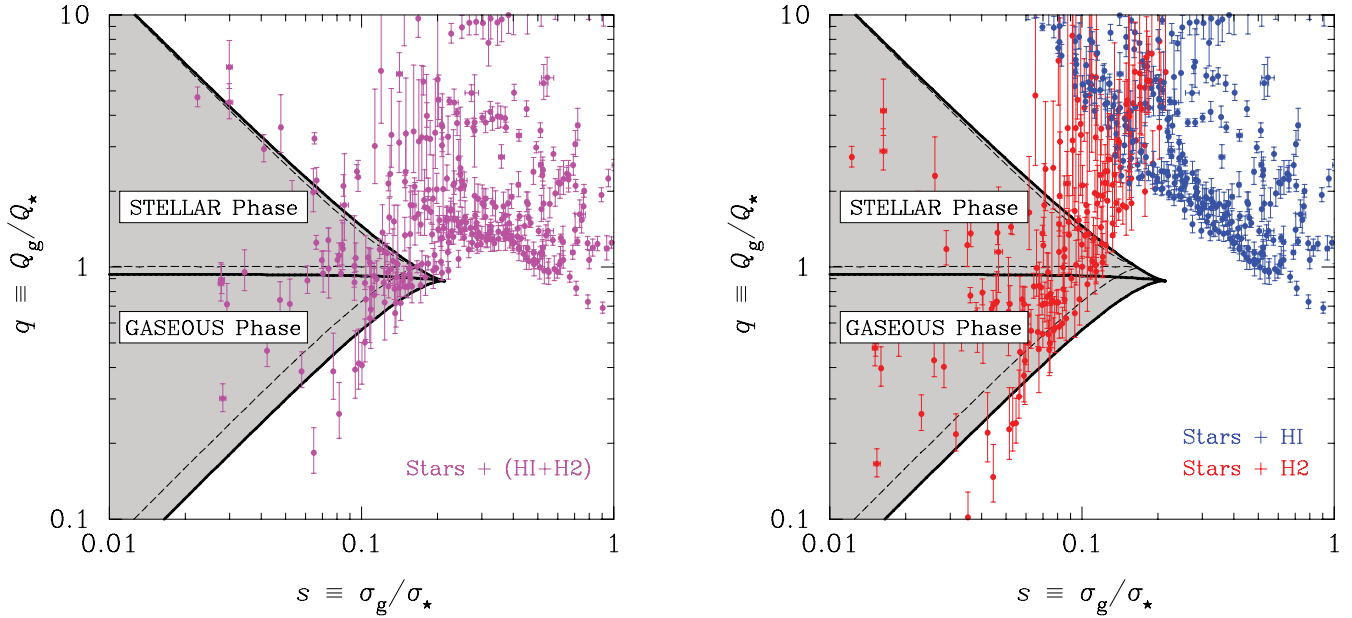
$$\frac{1}{Q_{R,N}} = \max\{SC_{R,N}(k)\}, \tag{11}$$

$$SC_{R,N}(k) = \frac{1}{Q_1} \frac{2K_1}{1 + K_1^2} + \sum_{i=2}^{N} \frac{1}{Q_i} \frac{2\left[1 - e^{-K_i^2} I_0\left(K_i^2\right)\right]}{K_i}, \tag{12}$$

$$K_i = k \frac{\sigma_i}{\kappa}, \tag{13}$$

$$Q_i = \frac{\kappa \sigma_i}{\pi G \Sigma_i}. \tag{14}$$

Let us illustrate how to find a simple, accurate, fast and more general Q diagnostic. In Section 2.1, we have shown that stars can be accurately treated as a fluid when evaluating Q. So we can safely replace the kinetic terms in equation (12) with their fluid

Figure 3. Why a multicomponent analysis is needed: the parameter plane of star–gas instabilities populated by THINGS spirals. The cases illustrated in the two panels are stars plus gas (left), and stars plus H I or H$_2$ (right). The galaxy data are from Leroy et al. (2008), Q_* and Q_g are the stellar and gaseous Toomre parameters, σ_* and σ_g are the relevant velocity dispersions of the two components. The shaded part of the (s, q) plane represents the condition for star–gas decoupling, with the stellar component treated as collisionless (thick solid lines) or collisional (thin dashed lines). This is the 'two-phase region' discussed in the text. The boundaries of this region and the transition line intersect at $(s, q) \simeq (0.21, 0.88)$ in the collisionless case, and at $(s, q) \simeq (0.17, 1)$ in the collisional case.

counterparts. We then face the heart of the problem: how to estimate the least stable wavenumber, k_{max}, without the usual maximization procedure. Consider the two-component case first, and compare the Romeo–Wiegert approximation (equations 9 and 10) with the two-fluid stability parameter (equations 6 and 7). One can easily infer that K_{max} fulfils the following conditions:

(i) If $Q_* > Q_g$, then $2K_{max}/(1 + K_{max}^2) \sim W$ and $2K_{max}s/(1 + K_{max}^2 s^2) \sim 1$. As $W = 2s/(1 + s^2)$, this implies that $K_{max} \sim 1/s$, i.e. $k_{max} \sim \kappa/\sigma_g$.

(ii) If $Q_g > Q_*$, then $2K_{max}/(1 + K_{max}^2) \sim 1$ and $2K_{max}s/(1 + K_{max}^2 s^2) \sim W$. This implies that $K_{max} \sim 1$, i.e. $k_{max} \sim \kappa/\sigma_*$.

Conditions (i) and (ii) have not been pointed out in previous analyses. They simply mean that $1/k_{max}$ is approximately the typical epicycle size of the less stable component. This approximation is not accurate when $s \approx 0.2$ and $q \approx 1$, since for such values there is a transition between three stability regimes and K_{max} has a jump across one of the interfaces (see discussion of Fig. 3). Note, however, that estimating K_{max} as above produces a very accurate estimate of Q_{Rf}, namely the Romeo–Wiegert approximation. This is because Q_{Rf} is continuous across the $q = 1$ line, and because the error that affects the estimate of Q_{Rf} is of second order with respect to that of K_{max}: $\Delta Q_{Rf} \propto (\Delta K_{max})^2$. The first-order term is obviously zero, since the first derivative of $SC_{Rf}(K)$ vanishes for $K = K_{max}$.[2] This flow of arguments suggests that we can estimate the N-component Q parameter as in the two-fluid case, i.e. by approximating $1/k_{max}$ with the typical epicycle size of the least stable component ($k_{max} \sim \kappa/\sigma_m$):

[2] This is actually the idea behind all minimization (or maximization) problems, and the reason why their solutions are robust. An instructive example is the 'optimal' Wiener filter used in signal/image processing (see, e.g., Press et al. 1992).

$$\frac{1}{Q_N} = \sum_{i=1}^{N} \frac{W_i}{Q_i}, \tag{15}$$

$$W_i = \frac{2\sigma_m \sigma_i}{\sigma_m^2 + \sigma_i^2}, \tag{16}$$

where the index m denotes the component with smallest Q: $Q_m = \min\{Q_i\}$. This is the component that dominates the local stability level ($W_m = 1$). All other components have less weight; the more σ_i differs from σ_m, the smaller the weight factor W_i.

What is the accuracy of Q_N? In Appendix A, we show how estimation uncertainties propagate from W_i to Q_N, and derive an upper bound for the resulting root-mean-square error:

$$\frac{\Delta Q_N}{Q_N} \lesssim 0.03 \sqrt{N}. \tag{17}$$

Equation (17) tells us that the accuracy of our approximation deteriorates slowly as we consider more and more components. In the case of greatest interest, stars plus H I plus H$_2$, the relative error is on average less than 6 per cent, i.e. almost as low as in the two-component case (see Fig. 2).

To demonstrate the accuracy of our approximation, we put it to a stringent test: the 10-component model of the solar neighbourhood analysed by Rafikov (2001). That model includes cold interstellar gas, giants, stars in six luminosity ranges, white and brown dwarfs. Rafikov also analysed the effect of varying the most uncertain model parameters. He motivated and discussed five cases, which we summarize in Appendix B. For each case, we compare Q_N with Rafikov's $Q_{R, N}$ parameter and compute the relative error $(Q_N - Q_{R, N})/Q_{R, N}$. Table 1 shows that our approximation is remarkably accurate. In all cases, the relative error is less than 5 per cent, which means twice as low as the upper bound predicted by equation (17).

Table 1. Accuracy of our approximation in the 10-component cases analysed by Rafikov (2001).

Case	$Q_{R,N}$	Q_N	$(Q_N - Q_{R,N})/Q_{R,N}$
1	1.10	1.12	1.8 per cent
2	1.00	1.04	3.7 per cent
3	1.00	1.04	4.5 per cent
4	1.00	1.01	0.8 per cent
4+1	1.00	1.01	1.2 per cent

$Q_{R,N}$ is the N-component Q parameter of Rafikov (2001), Q_N is our N-component Q parameter and $(Q_N - Q_{R,N})/Q_{R,N}$ is the relative error of our approximation.

2.3 Adding the effect of disc thickness

Our approximation is not yet complete. It does not include the stabilizing effect of disc thickness, which is important and should be taken into account when analysing the stability of galactic discs (Romeo & Wiegert 2011). In this section, we generalize the Romeo–Wiegert approach and provide a simple recipe for adding such an effect.

From the thin-disc limit, we have learned that the local stability level is dominated by the component with smallest Q (see equations 15 and 16). The contributions of the other components are weakened by the W_i factors, which are different and small if the components are dynamically distinct. In this case, we can estimate the effect of thickness reasonably well by considering each component separately. Romeo (1994) analysed this case in detail. The effect of thickness is to increase the stability parameter of each component by a factor T, which depends on the ratio of vertical to radial velocity dispersion:

$$T \approx \begin{cases} 1 + 0.6 \left(\dfrac{\sigma_z}{\sigma_R} \right)^2 & \text{for } 0 \lesssim \sigma_z/\sigma_R \lesssim 0.5, \\ 0.8 + 0.7 \left(\dfrac{\sigma_z}{\sigma_R} \right) & \text{for } 0.5 \lesssim \sigma_z/\sigma_R \lesssim 1. \end{cases} \quad (18)$$

Equation (18) can be inferred from fig. 3 (top) of Romeo (1994). The range $0 \lesssim \sigma_z/\sigma_R \lesssim 0.5$ is characteristic of the old stellar disc in Sc–Sd galaxies (Gerssen & Shapiro Griffin 2012), while $0.5 \lesssim \sigma_z/\sigma_R \lesssim 1$ is the usual range of velocity anisotropy (typical of the old stellar disc in Sa–Sbc galaxies, of young stars and the ISM). To approximate Q in this more general context, use then equation (15) with Q_i replaced by $T_i Q_i$:

$$\frac{1}{\mathcal{Q}_N} = \sum_{i=1}^{N} \frac{W_i}{T_i Q_i}, \quad (19)$$

where $\mathcal{Q}_N$ is our Q stability parameter for multicomponent and realistically thick discs, $Q_i = \kappa \sigma_i / \pi G \Sigma_i$ is the Toomre parameter of component i, T_i is given by equation (18) and W_i is given by equation (16). Note that the index m now denotes the component with smallest TQ: $T_m Q_m = \min \{T_i Q_i\}$. This is the component that dominates the local stability level. The contributions of the other components are still suppressed by the W_i factors.

2.4 What about the effect of ISM turbulence?

Turbulence plays a fundamental role in the dynamics and structure of cold interstellar gas (see, e.g., Elmegreen & Scalo 2004; McKee & Ostriker 2007; Agertz et al. 2009). The most basic aspect

of interstellar turbulence is the presence of supersonic motions. These are usually taken into account by identifying σ_g with the typical 1D velocity dispersion of the medium, rather than with its thermal sound speed. Another important aspect of interstellar turbulence is the existence of scaling relations between Σ_g, σ_g and the size of the region over which such quantities are measured (ℓ). Observations show that $\Sigma_{HI} \sim \ell^{1/3}$ and $\sigma_{HI} \sim \ell^{1/3}$ up to scales of 1–10 kpc, whereas $\Sigma_{H_2} \sim$ constant and $\sigma_{H_2} \sim \ell^{1/2}$ up to scales of about 100 pc (see, e.g., Elmegreen & Scalo 2004; McKee & Ostriker 2007; Romeo, Burkert & Agertz 2010).

Motivated by the large observational uncertainties of $\Sigma_g(\ell)$ and $\sigma_g(\ell)$, and having in mind near-future applications to high-redshift galaxies, Romeo et al. (2010) considered more general scaling relations, $\Sigma_g \propto \ell^a$ and $\sigma_g \propto \ell^b$, and explored the effect of turbulence on the gravitational instability of gas discs. They showed that turbulence excites a rich variety of stability regimes, several of which have no classical counterpart. See in particular the '*stability map of turbulence*' (fig. 1 of Romeo et al. 2010), which illustrates such stability regimes and populates them with observations, simulations and models of ISM turbulence. Hoffmann & Romeo (2012) extended this investigation to two-component discs of stars and gas, and analysed the stability of THINGS spirals. They showed that ISM turbulence alters the condition for star–gas decoupling and increases the least stable wavelength, but hardly modifies the Q parameter at scales larger than about 100 pc. Since these are the usual scales of interest, we do not include that effect in our approximation.

2.5 Application to THINGS spirals

Our approximation is now complete. Let us then show how to use our $\mathcal{Q}_N$ parameter for analysing the stability of galactic discs, and illustrate the strength of a multicomponent analysis.

In the following, we generalize the two-component approach of Romeo & Wiegert (2011). We consider the same sample of spiral galaxies as in Section 2.1 and refer to Leroy et al. (2008, hereafter L08), for a detailed description of the data and their translation into physical quantities. We treat stars, H I and H$_2$ as three components with the same surface densities and σ_* as in L08, but with distinct values of σ_g: $\sigma_{HI} = 11 \text{ km s}^{-1}$ (L08), and $\sigma_{H_2} = 6 \text{ km s}^{-1}$ (Wilson et al. 2011). For each galaxy, we compute the radial profile of $\mathcal{Q}_3$ using equation (19). We adopt $(\sigma_z/\sigma_R)_* = 0.6$, as was assumed by L08, and $(\sigma_z/\sigma_R)_{HI} = (\sigma_z/\sigma_R)_{H_2} = 1$, as is natural for collisional components. For comparison purposes, we also compute the radial profile of $\mathcal{Q}_2$, treating the ISM as a single component with $\Sigma_g = \Sigma_{HI} + \Sigma_{H_2}$ and $\sigma_g = 11 \text{ km s}^{-1}$ (L08).

Fig. 4 shows $\mathcal{Q}_3(R)$ and $\mathcal{Q}_2(R)$ for the whole galaxy sample. Note that the $\mathcal{Q}_3$ data are characterized by a sharp transition at about half the optical radius. For $R \lesssim 0.6 R_{25}$, $\mathcal{Q}_3$ spans a range of one order of magnitude, and a significant fraction of the data lie below or near the critical stability level (although in most of the cases $\mathcal{Q}_3 > 1$). For $R \gtrsim 0.6 R_{25}$, $\mathcal{Q}_3$ varies within a narrow range of values, and there is a single data point with $\mathcal{Q}_3 \leq 1$. Why do the inner and the outer discs of THINGS spirals have distinct stability properties? Why does the transition occur at about half the optical radius? To answer these questions, we have colour-coded the $\mathcal{Q}_3$ data so as to show which component dominates the local stability level. This is an important piece of information, which can easily be predicted using our $\mathcal{Q}_N$ diagnostic (see equation 19). The fundamental difference between inner and outer spiral discs is how H$_2$ contributes to disc (in)stability. For $R \lesssim 0.6 R_{25}$, H$_2$ dominates in one-third of the cases: it lowers the overall stability level, and increases the variance of $\mathcal{Q}_3$. At $R \approx 0.6 R_{25}$, the contribution of H$_2$ becomes negligible. Thus, H$_2$
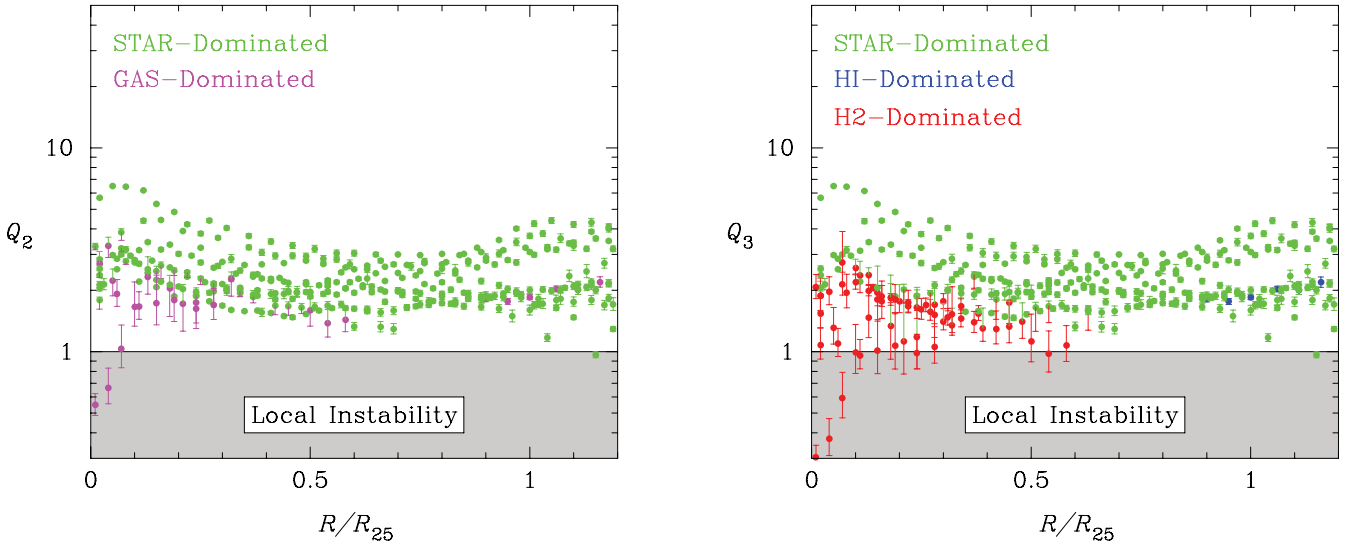
Figure 4. The stability level of THINGS spirals. The diagnostics used in the left- and right-hand panels are our $\mathcal{Q}_2$ and $\mathcal{Q}_3$ parameters (see equation 19 for $N = 2, 3$). The galaxy data are from Leroy et al. (2008), R is the galactocentric distance and R_{25} is the optical radius. The data are colour-coded so as to show whether the stability level is dominated by stars or gas (H I/H2), as predicted by equation (19). In the right-hand panel, the three data points that lie well below the critical stability level tell us that the nuclear region of NGC 6946 is subject to strong H2-dominated instabilities. This is consistent with the facts that NGC 6946 hosts a nuclear starburst (e.g. Engelbracht et al. 1996) and a nuclear 'bar within bar' (e.g. Fathi et al. 2007).

leaves a characteristic imprint on the stability of THINGS spirals, even though stars dominate in most of the cases. The contribution of H I is instead negligible everywhere, even at the edge of the optical disc, where H I is expected to contribute significantly. Such a stability scenario cannot be predicted by a two-component analysis. Note, in fact, that the $\mathcal{Q}_2$ data underestimate significantly how gas contributes to disc (in)stability, and fail to reproduce the transition at half the optical radius (compare the left- and right-hand panels of Fig. 4).

Fig. 5 illustrates how the stability properties of THINGS spirals vary with galactocentric distance. To extract such information, we

have binned the $\mathcal{Q}_3$ data of Fig. 4 in 12 rings of width $0.1 R/R_{25}$. For each ring, we have computed the median of $\mathcal{Q}_3$, the percentage of cases in which $\mathcal{Q}_3 < 1$ and how frequently each component dominates the local stability level. For comparison purposes, we have also binned the $\mathcal{Q}_2$ data and computed the corresponding stability characteristics. Note that H2 plays a primary role in disc (in)stability for $R \leq 0.1$–$0.2 R_{25}$, i.e. up to distances of about one disc scalelength ($R_{25} = 4.6 \pm 0.8 R_d$; L08). Thereafter, stars dominate more often. Note also that the frequency of H2-dominated cases decreases markedly with galactocentric distance, and falls below 10 per cent at $R = 0.5$–$0.6 R_{25}$. This corresponds to the transition
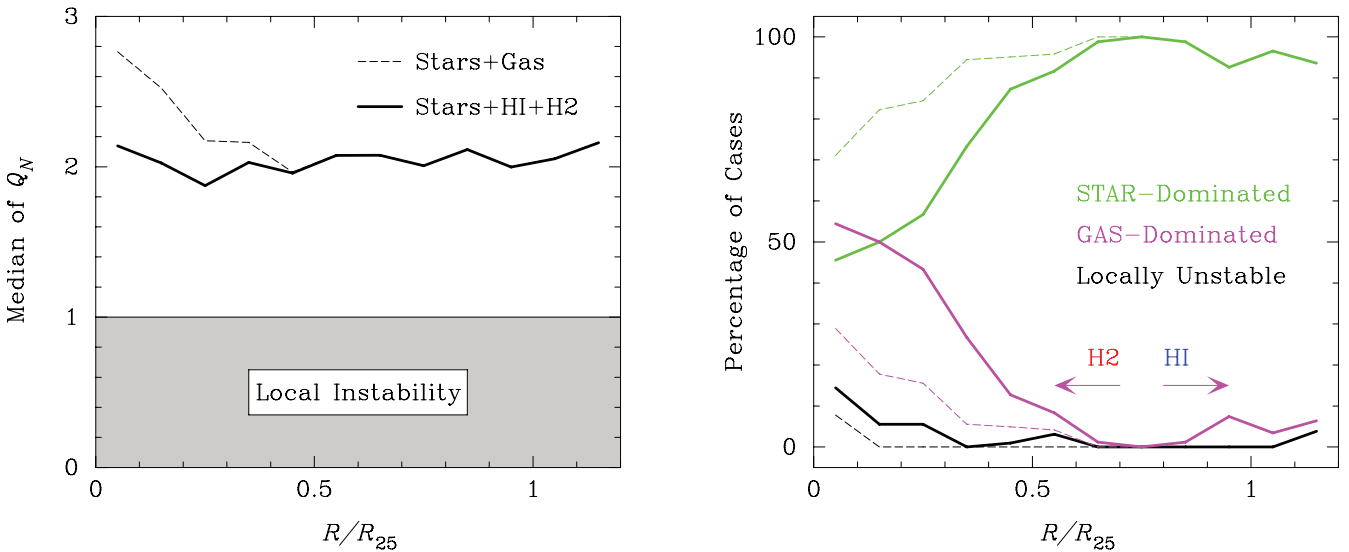

Figure 5. Stability characteristics of THINGS spirals. The radial profiles shown in the left- and right-hand panels are computed by binning the $\mathcal{Q}_N$ data of Fig. 4 in 12 rings of width $0.1 R/R_{25}$, where $\mathcal{Q}_N$ is our Q stability parameter for multicomponent and realistically thick discs (see equation 19 for $N = 2$, 3), R is the galactocentric distance and R_{25} is the optical radius. The right-hand panel shows how frequently the stability level is dominated by stars or gas (H I/H2), and how frequently $\mathcal{Q}_N < 1$. The thick solid lines are the predictions of a three-component analysis (stars plus H I plus H2), while the thin dashed lines represent the two-component case (stars plus gas).

radius identified in Fig. 4, and to the outskirts of the expected H_2 domain ($\Sigma_{H_2} \geq \Sigma_{H_I}$ for $R \leq 0.43 \pm 0.18\,R_{25}$; L08). The frequency of H I-dominated cases shows a tendency to increase for $R \geq 0.7$–$0.8\,R_{25}$, but it never rises above 10 per cent. The remaining stability characteristics provide more intriguing information. The frequency of locally unstable cases is below 10 per cent, except at distances smaller than about half the disc scalelength. The median of Q_3 lies well above the critical stability level, and is remarkably constant across the entire optical disc: $Q_{3\,med}(R) \simeq 2$ (see the left-hand panel of Fig. 5, and note the linear scale on the y-axis). Note, finally, how fast the two-component case diverges from the predicted radial profiles as we approach the galactic centre (compare the dashed and solid lines in the two panels of Fig. 5). This result illustrates, once again, (i) how important it is to treat stars, H I and H_2 as three distinct components when analysing the stability of galactic discs, and (ii) the strong advantage of using our Q_N parameter as a stability diagnostic.

3 DISCUSSION

Now that we have illustrated the strength of Q_N, let us remember its weaknesses. Like all Q parameters and stability criteria discussed so far, Q_N measures the stability of the disc against local axisymmetric perturbations, so it assumes that $kR \gg 1$. This is the short-wavelength approximation, which Binney & Tremaine (2008) define as 'an indispensable tool for understanding the properties of density waves in differentially rotating discs' (see p. 485 of Galactic Dynamics by Binney and Tremaine). Here, the relevant k is the least stable radial wavenumber, which can be approximated as $k_{max} \sim \kappa/\sigma_m$ (see Section 2).

Rather than estimating the magnitude and radial behaviour of $k_{max}R$ with qualitative arguments, we plot this quantity as a function of galactocentric distance for all THINGS spirals analysed in Section 2. Fig. 6 illustrates that the results of our stability analysis are consistent with the short-wavelength approximation. For
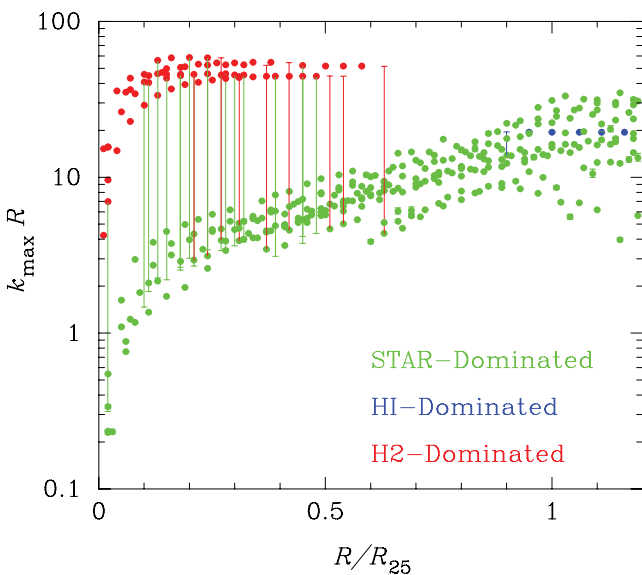
Figure 6. Consistency between the results of our stability analysis and the short-wavelength approximation, $k_{max}R \gg 1$, where k_{max} is the least stable radial wavenumber, R is the galactocentric distance and R_{25} is the optical radius. Large error bars signal a transition from star- to H_2-dominated regimes, or vice versa, which causes a jump in the value of k_{max} (see Section 2).

instance, the condition $k_{max}R > 3$ is fulfilled in 93 per cent of the cases, and is always true for $R \gtrsim 0.25\,R_{25} \approx R_d$, i.e. at distances larger than about one disc scalelength (remember that $R_{25} = 4.6 \pm 0.8\,R_d$; L08). In contrast, there are only 2 per cent of the data with $k_{max}R \leq 1$, all close to the galactic centre: $R \lesssim 0.05\,R_{25} \approx 0.25\,R_d$. Such data correspond to star-dominated regimes, which are more prone to violate the short-wavelength approximation since $k_{max} \sim \kappa/\sigma_*$ and $\sigma_* > \sigma_{H_I} > \sigma_{H_2}$. A comparison with the right-hand panel of Fig. 4 shows that the corresponding values of Q_3 are well above unity. As Q_3 is well above unity and star-dominated in most of the cases, the few data with $k_{max}R \leq 1$ do not have a significant influence on the stability of THINGS spirals. H I- and H_2-dominated regimes are fully consistent with the short-wavelength approximation, and so are the corresponding values of Q_3. In particular, the three data points that lie well below the critical stability level tell us that the nuclear region of NGC 6946 is subject to strong H_2-dominated instabilities (see again the right-hand panel of Fig. 4). This is consistent with the facts that NGC 6946 hosts a nuclear starburst (e.g. Engelbracht et al. 1996) and a nuclear 'bar within bar' (e.g. Fathi et al. 2007).

While the short-wavelength approximation is satisfied by most spiral galaxies, the assumption of axisymmetric (or tightly wound) perturbations is not so general. Local non-axisymmetric stability criteria are far more complex than Toomre's criterion: they depend critically on how tightly wound the perturbations are, and cannot generally be expressed in terms of a single 'effective' Q parameter (e.g. Lau & Bertin 1978; Morozov & Khoperskov 1986; Bertin et al. 1989b; Jog 1992; Lou & Fan 1998; Griv & Gedalin 2012). However, there is a general consensus that non-axisymmetric perturbations have a destabilizing effect, i.e. a disc with $Q \geq 1$ can still be locally unstable against such perturbations. Gas dissipation has a similar effect (Elmegreen 2011). These may be two of the reasons why the stability level of THINGS spirals is, on average, well above unity. The remarkable flatness of $Q_{3\,med}(R)$ across the entire optical disc is far more intriguing.

The assumption of local perturbations is quite controversial. While there is a general consensus that locally stable discs can be globally unstable as regards spiral structure formation, the dynamics and evolution of spiral structure depend critically on the radial profile of the Q stability parameter (e.g. Bertin et al. 1989a,b; Lowe et al. 1994; Romeo 1994; Korchagin et al. 2000, 2005; Khoperskov et al. 2007, 2012; Sellwood 2011). Our results about the stability level of THINGS spirals have no direct implications for that problem because they concern the THINGS sample as a whole, not each of the spirals. Useful constraints on the nature of spiral structure in galaxies might be found by analysing the radial profile of Q_N for each THINGS spiral, and by searching for trends in $Q_N(R)$ along the Hubble sequence. This is however well beyond the scope of this paper.

4 CONCLUSIONS

This paper provides a simple analytical recipe for estimating the Q stability parameter in multicomponent and realistically thick discs (see equation 19). Our Q_N parameter applies for any number of stellar and gaseous components ($i = 1, \ldots, N$), and for the whole range of velocity anisotropy observed in galactic discs: $0 \lesssim (\sigma_z/\sigma_R)_i \lesssim 1$. The accuracy of this approximation can be rigorously quantified in the thin-disc limit, where it scales as $N^{-1/2}$. For $N = 3$, the predicted root-mean-square error is well below 10 per cent. This is true even for larger values of N. For example, in the 10-component model(s) of the solar neighbourhood considered by Rafikov (2001) our

approximation is accurate to within 5 per cent. A further strength of the $\mathcal{Q}_N$ diagnostic is that it predicts which component dominates the local stability level. This is a useful piece of information, which should always be given when analysing the stability of galactic discs.

This paper also provides the first three-component analysis of THINGS spirals. Our analysis predicts how stars, H I and H_2 contribute to disc (in)stability, and how the stability properties of such galaxies vary with galactocentric distance. We show that H_2 plays a primary role up to distances of about one disc scalelength. Stars dominate thereafter, but the contribution of H_2 remains significant even at distances as large as half the optical radius. This is in sharp contrast to the role played by H I, which is negligible up to the edge of the optical disc. We also show that the stability level of THINGS spirals is, on average, remarkably flat and well above unity.

REFERENCES

Agertz O., Lake G., Teyssier R., Moore B., Mayer L., Romeo A. B., 2009, MNRAS, 392, 294
Bertin G., Lin C. C., 1996, Spiral Structure in Galaxies: A Density Wave Theory. The MIT Press, Cambridge
Bertin G., Romeo A. B., 1988, A&A, 195, 105
Bertin G., Lin C. C., Lowe S. A., Thurstans R. P., 1989a, ApJ, 338, 78
Bertin G., Lin C. C., Lowe S. A., Thurstans R. P., 1989b, ApJ, 338, 104
Bevington P. R., Robinson D. K., 2003, Data Reduction and Error Analysis for the Physical Sciences. McGraw-Hill, Boston
Binney J., Tremaine S., 2008, Galactic Dynamics. Princeton Univ. Press, Princeton, NJ
Cacciato M., Dekel A., Genel S., 2012, MNRAS, 421, 818
Ceverino D., Dekel A., Bournaud F., 2010, MNRAS, 404, 2151
Dalcanton J. J., Yoachim P., Bernstein R. A., 2004, ApJ, 608, 189
Dekel A., Sari R., Ceverino D., 2009, ApJ, 703, 785
Elmegreen B. G., 1995, MNRAS, 275, 944
Elmegreen B. G., 2011, ApJ, 737, 10
Elmegreen B. G., Scalo J., 2004, ARA&A, 42, 211
Elson E. C., de Blok W. J. G., Kraan-Korteweg R. C., 2012, AJ, 143, 1
Engelbracht C. W., Rieke M. J., Rieke G. H., Latter W. B., 1996, ApJ, 467, 227
Fathi K., Toonen S., Falcón-Barroso J., Beckman J. E., Hernandez O., Daigle O., Carignan C., de Zeeuw T., 2007, ApJ, 667, L137
Forbes J., Krumholz M., Burkert A., 2012, ApJ, 754, 48
Gerssen J., Shapiro Griffin K., 2012, MNRAS, 423, 2726
Griv E., Gedalin M., 2012, MNRAS, 422, 600
Hoffmann V., Romeo A. B., 2012, MNRAS, 425, 1511
Jog C. J., 1992, ApJ, 390, 378
Jog C. J., 1996, MNRAS, 278, 209
Jog C. J., Solomon P. M., 1984a, ApJ, 276, 114
Jog C. J., Solomon P. M., 1984b, ApJ, 276, 127
Khoperskov A. V., Just A., Korchagin V. I., Jalali M. A., 2007, A&A, 473, 31
Khoperskov S. A., Khoperskov A. V., Khrykin I. S., Korchagin V. I., Casetti-Dinescu D. I., Girard T., van Altena W., Maitra D., 2012, MNRAS, 427, 1983
Kim W.-T., Ostriker E. C., 2007, ApJ, 660, 1232
Korchagin V., Kikuchi N., Miyama S. M., Orlova N., Peterson B. A., 2000, ApJ, 541, 565
Korchagin V., Orlova N., Kikuchi N., Miyama S. M., Moiseev A., 2005, preprint (arXiv:astro-ph/0509708)
Lau Y. Y., Bertin G., 1978, ApJ, 226, 508
Leroy A. K., Walter F., Brinks E., Bigiel F., de Blok W. J. G., Madore B., Thornley M. D., 2008, AJ, 136, 2782 (L08)
Li Y., Mac Low M.-M., Klessen R. S., 2005, ApJ, 626, 823
Li Y., Mac Low M.-M., Klessen R. S., 2006, ApJ, 639, 879
Lin C. C., Shu F. H., 1966, Proc. Natl. Acad. Sci. USA, 55, 229
Lou Y.-Q., Fan Z., 1998, MNRAS, 297, 84
Lowe S. A., Roberts W. W., Yang J., Bertin G., Lin C. C., 1994, ApJ, 427, 184
Mastropietro C., Burkert A., Moore B., 2009, MNRAS, 399, 2004
McKee C. F., Ostriker E. C., 2007, ARA&A, 45, 565
Meurer G. R., Zheng Z., de Blok W. J. G., 2013, MNRAS, 429, 2537
Morozov A. G., 1981, SvA, 7, L5
Morozov A. G., Khoperskov A. V., 1986, Ap, 24, 266
Press W. H., Teukolsky S. A., Vetterling W. T., Flannery B. P., 1992, Numerical Recipes in Fortran: The Art of Scientific Computing. Cambridge Univ. Press, Cambridge
Rafikov R. R., 2001, MNRAS, 323, 445
Robertson B. E., Kravtsov A. V., 2008, ApJ, 680, 1083
Romeo A. B., 1985, Stabilità di Sistemi Stellari in Presenza di Gas: Fenomeni Collettivi in Sistemi Autogravitanti a Due Componenti. Tesi di Laurea, University of Pisa and Scuola Normale Superiore, Pisa, Italy
Romeo A. B., 1990, PhD thesis, SISSA
Romeo A. B., 1992, MNRAS, 256, 307
Romeo A. B., 1994, A&A, 286, 799
Romeo A. B., Wiegert J., 2011, MNRAS, 416, 1191
Romeo A. B., Burkert A., Agertz O., 2010, MNRAS, 407, 1223
Sellwood J. A., 2011, MNRAS, 410, 1637
Shadmehri M., Khajenabi F., 2012, MNRAS, 421, 841
Shen Y., Lou Y.-Q., 2003, MNRAS, 345, 1340
Shu F. H., 1968, PhD thesis, Harvard Univ.
Toomre A., 1964, ApJ, 139, 1217
Watson L. C., Martini P., Lisenfeld U., Wong M.-H., Böker T., Schinnerer E., 2012, ApJ, 751, 123
Westfall K. B., Bershady M. A., Verheijen M. A. W., Andersen D. R., Martinsson T. P. K., Swaters R. A., Schechtman-Rook A., 2011, ApJ, 742, 18
Williamson D. J., Thacker R. J., 2012, MNRAS, 421, 2170
Wilson C. D. et al., 2011, MNRAS, 410, 1409
Yang C.-C., Gruendl R. A., Chu Y.-H., Mac Low M.-M., Fukui Y., 2007, ApJ, 671, 374
Yim K., Wong T., Howk J. C., van der Hulst J. M., 2011, AJ, 141, 48
Zheng Z., Meurer G. R., Heckman T. M., Zwaan M., 2013, MNRAS, submitted

APPENDIX A: DERIVATION OF EQUATION (17)

From standard error analysis, we know that the relative uncertainty of Q_N is approximately equal to that of $1/Q_N$:

$$\frac{\Delta Q_N}{Q_N} \sim \frac{\Delta(1/Q_N)}{1/Q_N} \tag{A1}$$

(see, e.g., Bevington & Robinson 2003). We also know that $\Delta(1/Q_N)$ arises from estimation uncertainties in W_i (see equation 15). If we assume that all ΔW_i are uncorrelated and of comparable magnitude, then the error propagation equation reduces to

Table B1. Rafikov's reference model of the solar neighbourhood: surface densities and velocity dispersions of the various components.

i	Component	Σ_i (M$_\odot$ pc^{-2})	σ_i (km s^{-1})
1	ISM	13.0	7.0
2	Giants	0.4	26.0
3	$M_V < 2.5$	0.9	17.0
4	$2.5 < M_V < 3.0$	0.6	20.0
5	$3.0 < M_V < 4.0$	1.1	22.5
6	$4.0 < M_V < 5.0$	2.0	26.0
7	$5.0 < M_V < 8.0$	6.5	30.5
8	$M_V > 8.0$	12.3	32.5
9	White dwarfs	4.4	32.5
10	Brown dwarfs	6.2	32.5

$$\Delta(1/Q_N) \sim \Delta W \left(\sum_{i=1}^{N} \frac{1}{Q_i^2} \right)^{1/2} . \tag{A2}$$

Remembering that $Q_i \geq Q_m$, we get

$$\Delta(1/Q_N) \lesssim \frac{\Delta W}{Q_m} \sqrt{N} . \tag{A3}$$

Noting that $1/Q_N > 1/Q_m$ and using equation (A1), we then find

$$\frac{\Delta Q_N}{Q_N} \lesssim \Delta W \sqrt{N} . \tag{A4}$$

ΔW can be evaluated from the two-component case, where the root-mean-square value of the relative error $(Q_2 - Q_{\rm Rk})/Q_{\rm Rk}$ is 5 per cent (see Fig. 2). Setting $\Delta W \sqrt{2} \approx 0.05$, we finally obtain $\Delta W \approx 0.03$ and thus

$$\frac{\Delta Q_N}{Q_N} \lesssim 0.03 \sqrt{N} . \tag{A5}$$

APPENDIX B: THE 10-COMPONENT CASES ANALYSED BY RAFIKOV (2001)

(i) *Case 1:* Rafikov's reference model of the solar neighbourhood. The epicyclic frequency is $\kappa = 36$ km s^{-1} kpc^{-1}. The surface densities and velocity dispersions of the various components are listed in Table B1.

(ii) *Case 2:* same as Case 1, but with the velocity dispersion of white and brown dwarfs decreased from 32.5 to 20.0 km s^{-1}.

(iii) *Case 3:* same as Case 1, but with the total surface density of white and brown dwarfs increased from 10.6 to 25.0 M$_\odot$ pc^{-2}.

(iv) *Case 4:* same as Case 1, but with the gas velocity dispersion decreased from 7.0 to 5.9 km s^{-1}.

(v) *Case 4+1:* same as Case 1, but with the gas surface density increased from 13.0 to 14.8 M$_\odot$ pc^{-2} (this case was only mentioned by Rafikov).

This paper has been typeset from a TeX/LaTeX file prepared by the author.